Joint focusing inversion of marine controlled-source electromagnetic and full tensor gravity gradiometry data: case study of the Nordkapp Basin in Barents Sea, Norway

*Xiaolei Tu *, and Michael S. Zhdanov, Consortium for Electromagnetic Modeling and Inversion, University of Utah, and TechnoImaging*

Summary

Geophysical studies for offshore exploration have long been dominated by seismic methods. With the frontier areas of hydrocarbon exploration moving to more challenging geological settings, decisions based on seismic methods alone could be risky. Independent information from alternative geophysical methods integrated with seismic data becomes essential and necessary in this challenging situation. We consider an approach of integrating the complementary information of different geophysical methods to obtain self-consistent geophysical models based on using joint focusing stabilizers in regularized joint inversion of multiphysics data. The method enforces strong coupling between different models and promotes the sharp boundaries of the targets. The practical effectiveness of the developed methods is demonstrated by the case study of integrating and imaging electromagnetic (EM) and full tensor gravity gradiometry (FTG) data collected in the Nordkapp Basin in Barents Sea, Norway.

Introduction

Over the last decades, marine controlled-source electromagnetic (MCSEM), magnetotelluric (MT), as well as potential field methods, have found applications in offshore oil and gas exploration (Flosadottir and Constable, 1996; Constable, 2010; Andreis and MacGregor, 2011; Hokstad et al., 2011; Stadtler et al., 2014; Miller et al., 2019). In an MCSEM survey, electric current is injected into the seawater from an underwater electric bipole source, towed behind the ship. Simultaneously, an array of receivers, either towed by the same ship or seated on the seafloor, records the induced electromagnetic (EM) signals (Zhdanov, 2009, 2010; Constable, 2010; Mattsson and Anderson, 2010; Constable et al., 2016). The subsurface resistivity information is inferred from analyzing the recorded EM signals. The EM data are sensitive to resistive structures, such as gas- or oil-saturated reservoirs, basalt traps, and salt caps, whose resistivity could reach several hundred or thousand Ohm-m, more resistive than the sediments by one or two orders of magnitude (Constable, 2010; Moorkamp et al., 2016). Potential fields are usually used to estimate the depth to the basement and are also employed in salt imaging (Stadtler et al., 2014; Tu and Zhdanov, 2019).

A common issue with EM and potential field methods, however, is that their sensitivities decrease rapidly with the increasing of depth, making the inverse problem extremely challenging. Since different geophysical data are sensitive to different physical properties (i.e., resistivity or density contrast) and may contain complementary information of the subsurface, joint inversion of EM and potential fields could enhance the images of subsurface and reduce the uncertainties of generated geophysical models.

Several approaches to joint inversion have been developed over the last decades. They can be classified into two categories, namely, petrophysical and structural approaches. (e.g., Gao et al., 2012; Sun and Li 2017; Gallardo and Meju, 2004, 2007; Miller et al., 2019). A unified approach to joint inversion based on Gramian constraints was also developed recently (Zhdanov et al., 2012; Zhdanov, 2015). It could be demonstrated that the petrophysical and structural methods are special cases of the Gramian approach. These methods usually generate smooth and fuzzy models when applied to EM or potential fields, due to the fields' diffusive nature. In scenarios where high contrasts of geophysical properties present, e.g., salt imaging, focused models with sharp boundaries are favorable. A joint inversion method that could promote focused images is essential for EM and potential field methods.

We have developed a framework for joint inversion of multi-physics data based on the joint minimum support (JMS) functional introduced in Molodsov and Troyan (2017) and Zhdanov and Cuma (2018). The proposed method (1) enforces structural similarity between different model parameters through minimizing a JMS stabilizer; (2) promotes the focused image and sharp boundaries of the anomalous body; and (3) does not introduce over coupling artifact. We have carefully tested the proposed method with synthetic models by jointly inverting the MCSEM and FTG data. We have also applied the developed methods in a case study of interpreting multi-physics data collected in the Nordkapp Basin, Barents Sea, Norway.

Theory

We represent the corresponding forward modeling problems for MCSEM and FTG data with following operator equations:

$$\boldsymbol{d}^{(j)} = \mathbf{A}^{(j)}\left(\mathbf{m}^{(j)}\right), \qquad j = 1,2,$$

where $d^{(1)}$and $d^{(2)}$ represent the MCSEM and FTG data; $\mathbf{m}^{(1)}$ and $\mathbf{m}^{(2)}$ are the sea-bottom conductivity and density distributions. $\mathbf{A}^{(1)}$ and $\mathbf{A}^{(2)}$ denote the forward operators for EM and gravity fields, respectively. In this project we use the integral equation (IE) method for EM modeling. The IE method is most effective for modeling the EM response from the localized anomalous bodies embedded in a layered background. In a marine environment, the sediment layers

10.1190/segam2021-3581155.1

are usually flat, making it an ideal application scenario for the IE method. The gravity forward modeling problem is solved with the point mass approximation method. Both the EM and FTG forward modeling algorithms are fully parallelized with Message Passing Interface (MPI) and OpenMP to speed up the computation and to reduce the required computer memory, which is crucial for joint inversion calculation. For implementation details, we refer to Cuma et al. (2012) and Tu and Zhdanov (2019).

The joint inversion of MCSEM and FTG data is performed by minimizing the parametric (objective) functional:

$$P = \sum_{j=1}^{2} \phi^{(j)}(\mathbf{m}^{(j)}) + \sum_{j=1}^{2} \alpha^{(j)} \psi^{(j)}(\mathbf{m}^{(j)}) + \beta S_{JMS}(\mathbf{m}^{(1)}, \mathbf{m}^{(2)}),$$

where $\phi^{(j)}$ denotes the misfit functional for the j-th type of data; $\psi^{(j)}$ represents the regularization stabilizer promoting preferred structures of the model; $\alpha^{(j)}$ and β are the regularization parameters balancing the misfits and the corresponding stabilizers.

$s_{JMS}\left(m^{(1)}, m^{(2)}\right)$ is the joint minimum support (JMS) stabilizer of Zhdanov and Cuma (2018). The JMS functional of two model parameters $\mathbf{m}^{(1)}$ and $\mathbf{m}^{(2)}$ is calculated as follows:

$$S_{JMS}\left(\mathbf{m}^{(1)}, \mathbf{m}^{(2)}\right) = \int_V \frac{\sum_{j=1}^{2}\left(\widetilde{m}^{(j)} - \widetilde{m}_{apr}^{(j)}\right)^2}{\sum_{j=1}^{2}\left(\widetilde{m}^{(j)} - \widetilde{m}_{apr}^{(j)}\right)^2 + e^2},$$

where $\widetilde{m}^{(j)}$ denotes some transform (e.g., logarithm) of the original model parameter, $\mathbf{m}^{(j)}$, to make the values of the two transformed model parameters to be properly scaled. We use logarithmic conductivity and coupled logarithmic conductivity and density contrast in the joint inversion.

The JMS functional is proportional to the joint support of model parameters, i.e., the volume of the subdomain where at least one of the model parameters deviates from the background or a priori model. The JMS stabilizer enforces both structural similarities between the two models and the sharp boundaries of the anomalies.

Considering that the probability density functions of data and model uncertainties are usually long-tailed distributed (Claerbout and Muir, 1973), we know that the least-squares L2 error metric based on Gaussian uncertainty assumption may lead to biased models (Tarantola, 2005b). This issue is of significant importance for MCSEM survey, which always contains extremely noisy data at long offsets. The error metrics less sensitive to large measurement errors and more appropriate to long-tailed probability density functions could yield far more stable estimation of the model parameters than the L2 norm (Guitton and Symes, 2003). In our study, we employ the robust norms for the misfit functional:

$$\phi^{(j)}(\mathbf{m}^{(j)}) = \left\| \mathbf{W}_d^{(j)} \left[\mathbf{A}^{(j)}\left(\mathbf{m}^{(j)}\right) - \mathbf{d}_o^{(j)} \right] \right\|_\rho^2,$$

where $W_d^{(j)}$ represents the corresponding data weights; $d_o^{(j)}$ are the observed data, i.e., MCSEM or FTG data; $||\cdot||_\rho^2$ denotes the robust norm, e.g., Huber or Bisquare norm. The robust norms could be easily represented as quasi-quadratic functionals (Tu and Zhdanov, 2020), making it convenient to optimize.

We could also incorporate a priori information into the inversion using the minimum norm (MN) stabilizer,

$$\psi^{(i)}\left(\mathbf{m}^{(j)}\right) = \left\| \mathbf{W}_m^{(j)} \left(\mathbf{m}^{(j)} - \mathbf{m}_{apr}^{(j)} \right) \right\|^2,$$

which would favor a model close to the a priori model $\mathbf{m}_{apr}^{(j)}$. The MN stabilizer requires a relatively smooth behavior of the model, leading to the simplest model structures. The model weights $W_m^{(j)}$ and data weights $W_d^{(j)}$ are determined based on the integrated sensitivity (Zhdanov, 2002, 2015), to provide an equal sensitivity of the different components of observed data to the cells located at different depths and horizontal positions.

We solve the minimization problem using the reweighted regularized conjugate gradient (RRCG) method. Implementation details of the method could be found in Zhdanov (2015).

Case study: joint inversion of the MCSEM and FTG data collected in the Nordkapp Basin of Barents Sea

We have inverted the data collected over an area of the Nordkapp Basin (NKB) in the Western Barents Sea. The survey area is characterized by a wide distribution of salt which dramatically affected the petroleum system's evolution in the NKB. Seismically imaging the salt was proved to be extremely difficult due to weak primaries, strong multiples and diffractions, and a small impedance contrast at base salt. According to Hokstad et al. (2011), imaging in the rim synclines is good, but the salt structures are surrounded by a seismic shadow zone where the interpretation becomes difficult.

In order to address these difficulties, StatoilHydro commissioned Bell Geospace in 2008 to conduct a 3D ship-borne FTG survey in the NKB area with line spacing of 25 m. Later on, EMGS on behalf of Equinor conducted a MCSEM survey over the same area.

We present the example of the joint inversion of the MCSEM and FTG data acquired over the Uranus salt diapir in the NKB. The MCSEM data were collected by 27 receivers arranged in two survey lines. The positions of the receivers and the transmitter lines on a map of gravity data are shown in Figure 1. The data contained inline electric fields at two frequencies of 1 and 3 Hz. Three components of the FTG data, Gxx, Gyy, and Gzz, were used for the gravity inversions

Joint focusing inversion of marine controlled-source electromagnetic and gravity gradiometric data: case study of the Nordkapp Basin in Barents Sea, Norway

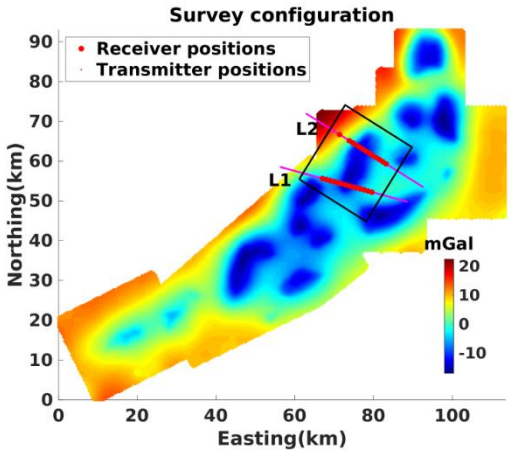

Figure 1: MCSEM survey configuration in NKB overlaid on a map of gravity data. The thick black box outlines the inversion domain.

We first separately inverted the MCSEM data with a hybrid stabilizer incorporating y-directed smoothing and focusing (Zhdanov, 2015). We also inverted the FTG data separately with a focusing stabilizer and produced a result similar to those of Xu et al, 2020. We then applied the developed method of joint focusing inversion to the MCSEM and FTG data. Both separate and joint inversions converged to the same level of misfit, approximately, the data's noise level.

The vertical profiles, corresponding to the two MCSEM survey lines, L1 and L2, are presented in Figures 2 and 3, respectively. The Uranus salt is reasonably imaged by both the separate and joint inversions. However, the joint inversion generates more focused images of it, and therefore delineates its boundaries, especially the salt base much better. The salt base across L1 line is estimated as between 3000 m to 3500 m. Due to the edge effect, the separately inverted density model presents density-lows on both edges of the X inversion domain. These artifacts, however, are eliminated through joint inversion. Besides, the density highs are guided by the conductors of the resistivity model. These conductors and density-highs are interpreted as sediments.

We finally present comparisons of the joint inverted resistivity and density models with a seismic image profile (Hokstad et al., 2011) in Figure 4. The conductors and density-highs between the depth of 1 km to 2 km are aligned with the seismic horizons, which are interpreted as the Jurassic sediments (Stadtler et al., 2014). Another pronounced feature is a weak conductive and weak dense anomaly below 3 km depth with the x-coordinate between -4 km to -1 km, which coincides with the mini basin identified from the seismic profile.

Conclusion

We have implemented a method of joint inversion for multi-physics data based on the joint minimum support (JMS) stabilizer. The developed method promotes structural similarity between different model parameters and the sharp boundaries of the anomalous bodies. At the same time, the method could decouple the model parameters when necessary, without introducing over-coupling artifacts.

The developed method has been applied to the joint inversion of MCSEM and FTG data. We have carefully tested the method with synthetic models and have applied it to multi-physics data collected in the Nordkapp Basin, Barents Sea, Norway. The case study has demonstrated the practical effectiveness of the developed method in imaging the sea-bottom salt structures.

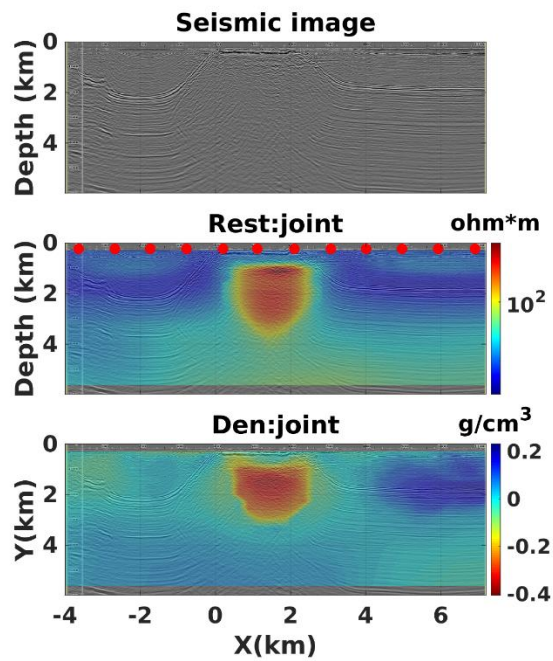

Figure 4: Comparison of the joint inverted resistivity and density models with seismic image across profile L1.

Acknowledgements

The authors thank the Consortium for Electromagnetic Modeling and Inversion (CEMI) at the University of Utah and TechnoImaging for support of this research. The MCSEM and FTG data were collected by EMGS and BellGeospace and made available by the Equinor (former Statoil). We also thank Dr. Ketil Hokstad from Equinor for his valuable suggestions on MCSEM data processing.

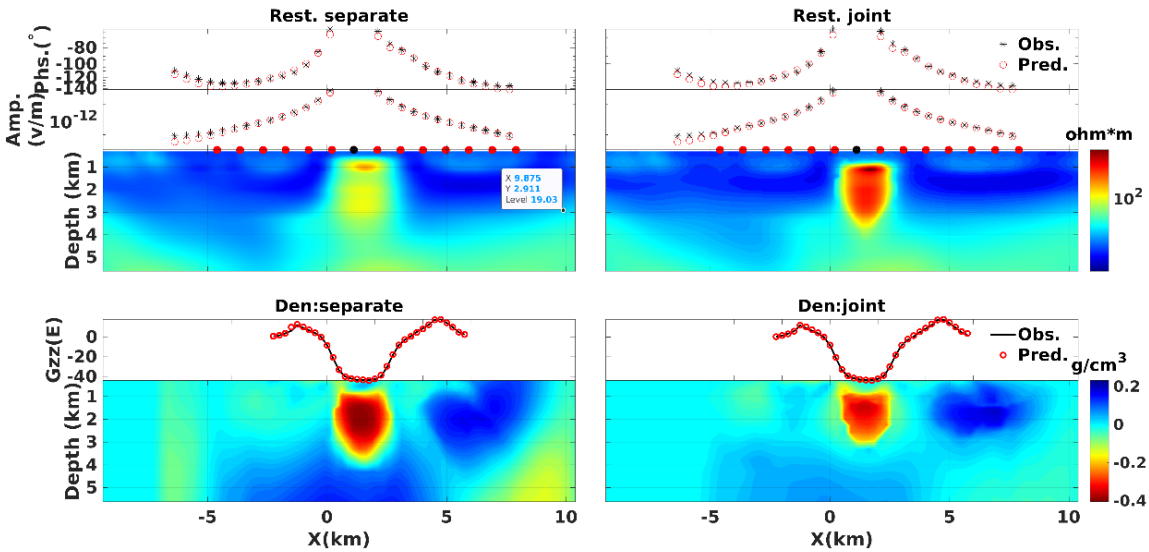

Figure 2: Profile L1 of inverted resistivity (top) and density (bottom) models. The left panels show the results of standalone inversions, while the right panels present the joint inversion results. The MCSEM receiver positions are shown as dots in the top panels. The phase and amplitude of a CRG EM data are shown on top of the resistivity models. The predicted and observed Gzz components of the FTG data across L1 line are plotted above the density models.

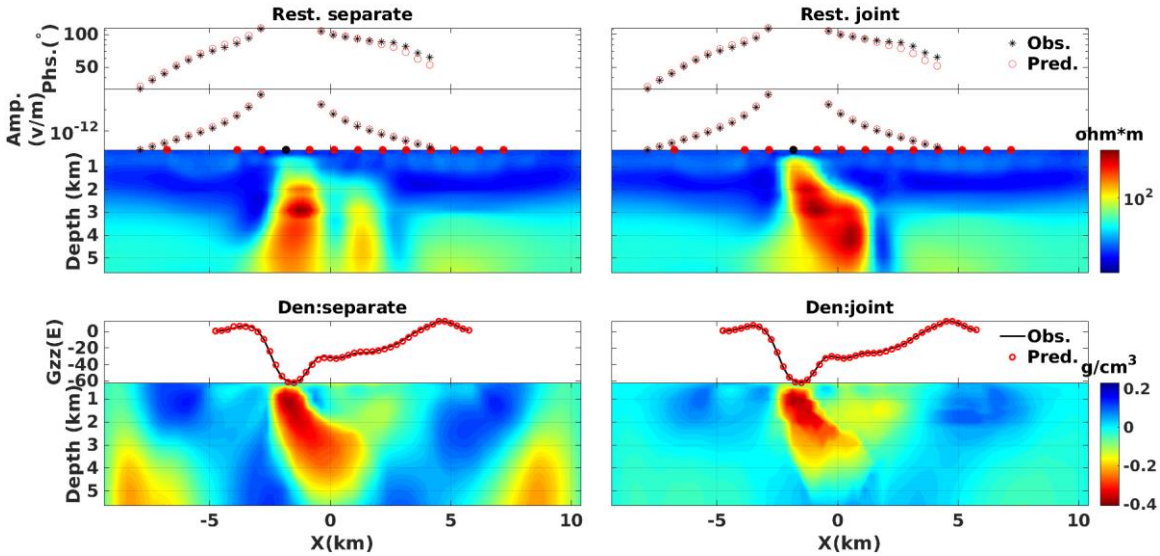

Figure 3: Profile L2 of inverted resistivity (top) and density (bottom) models. The left panels show the results of standalone inversions, while the right panels present the joint inversion results.

REFERENCES

Andreis, D., and L. MacGregor, 2011, Using csem to monitor production from a complex 3d gas reservoir|a synthetic case study: The Leading Edge, **30**, 1070–1079, doi: https://doi.org/10.1190/1.3640531.

Claerbout, J. F., and F. Muir, 1973, Robust modeling with erratic data: Geophysics, **38**, 826–844, doi: https://doi.org/10.1190/1.1440378.

Constable, S., 2010, Ten years of marine csem for hydrocarbon exploration: Geophysics, **75**, 75A67–75A81, doi: https://doi.org/10.1190/1.3483451.

Constable, S., P. K. Kannberg, and K. Weitemeyer, 2016, Vulcan: A deep-towed csem receiver: Geochemistry, Geophysics, Geosystems, **17**, 1042–1064, doi: https://doi.org/10.1002/2015GC006174.

Cuma, M., G. A. Wilson, and M. S. Zhdanov, 2012, Large-scale 3D inversion of potential field data: Geophysical Prospecting, **60**, 1186–1199, doi: https://doi.org/10.1111/j.1365-2478.2011.01052.x.

Flosadottir, A. H., and S. Constable, 1996, Marine controlled-source electromagnetic sounding: 1. modeling and experimental design: Journal of Geophysical Research: Solid Earth, **101**, 5507–5517, doi: https://doi.org/10.1029/95JB03739.

Gallardo, L. A., and M. A. Meju, 2004, Joint two-dimensional dc resistivity and seismic travel time inversion with cross- gradients constraints: Journal of Geophysical Research: Solid Earth, **109**, doi: https://doi.org/10.1029/2003JB002716.

Gao, G., A. Abubakar, and T. M. Habashy, 2012, Joint petrophysical inversion of electromagnetic and full-waveform seismic data: Geophysics, **77**, WA3–WA18, doi: https://doi.org/10.1190/geo2011-0157.1.

Guitton, A., and W. W. Symes, 2003, Robust inversion of seismic data using the Huber norm: Geophysics, **68**, 1310–1319, doi: https://doi.org/10.1190/1.1598124.

Hokstad, K., B. Fotland, G. Mackenzie, V. Antonsdottir, S.-K. Foss, C. Stadtler, C. Fichler, M. Haverl, B. M. T. Waagan, E. A. Myrlund, L. Masnaghetti, F. Ceci, and P.-Y. Raya, 2011, Joint imaging of geophysical data: Case history from the Nordkapp Basin, Barents Sea: 1098–1102, doi: https://doi.org/10.1190/1.3627395.

Mattsson, J., and C. Anderson, 2010, An integrated approach to marine electromagnetic surveying using a towed streamer and source: First Break, **28**, doi: https://doi.org/10.3997/1365-2397.28.5.38986.

Miller, R. V., M. A. Meju, A. S. Saleh, R. L. Mackie, and F. Miorelli, 2019, Structureguided 3D joint inversion of CSEM and MT data from a fold-thrust belt: 1115–1119, doi: https://doi.org/10.1190/segam2019-3216157.1.

Molodtsov, D., and V. Troyan, 2017, Multiphysics joint inversion through joint sparsity regularization: SEG Technical Program Expanded Abstracts, 1262–1267, doi: https://doi.org/10.1190/segam2017-17792589.1.

Moorkamp, M., B. Heincke, M. Jegen, R. W. Hobbs, and A. W. Roberts, 2016, Joint nversion in Hydrocarbon Exploration: American Geophysical Union (AGU), 167–189, doi: https://doi.org/10.1190/geo2017-0112.1.

Stadtler, C., C. Fichler, K. Hokstad, E. A. Myrlund, S. Wienecke, and B. Fotland, 2014, Improved salt imaging in a basin context by high resolution potential field data: Nordkapp basin, barents sea: Geophysical Prospecting, **62**, 615–630, doi: https://doi.org/10.1111/1365-2478.12101.

Sun, J., and Y. Li, 2017, Joint inversion of multiple geophysical and petrophysical data using generalized fuzzy clustering algorithms: Geophysical Journal International, **208**, 1201–1216, doi: https://doi.org/10.1093/gjihttps://doi.org//ggw442.

Tarantola, A., 2005, Inverse problem theory and methods for model parameter estimation, in Society for Industrial and Applied Mathematics, Other titles in applied mathematics, doi: https://doi.org/10.1137/1.9780898717921.

Tu, X., and M. S. Zhdanov, 2019, Enhancement and Sharpening the Migration Images of the Gravity Field and Its.

Tu, X., and M. S. Zhdanov, 2020, Robust Synthetic Aperture Imaging of Marine Controlled-source Electromagnetic Data: IEEE Transactions on Geoscience and Remote Sensing, doi: https://doi.org/10.1109/TGRS.2020.2966727.

Xu, Z., L. Wan, and M. S. Zhdanov, 2020, Focusing iterative migration of gravity gradiometry data acquired in the Nordkapp Basin, Barents Sea: Geophysical Prospecting, **68**, 2292–2306, doi: https://doi.org/10.1111/1365-2478.12990.

Zhdanov, M. S., 2002, Geophysical inverse theory and regularization problems: Elsevier Science.

Zhdanov, M. S., 2009, Geophysical electromagnetic theory and methods: Elsevier Science.

Zhdanov, M. S., 2010, Electromagnetic geophysics: Notes from the past and the road ahead: Geophysics, **75**, 75A49–75A66, doi: https://doi.org/10.1190/1.3483901.

Zhdanov, M. S., 2015, Inverse theory and applications in geophysics, 2nd Ed.: Elsevier, doi: https://doi.org/10.1016/C2012-0-03334-0.

Zhdanov, M. S., A. Gribenko, and G. Wilson, 2012, Generalized joint inversion of multimodal geophysical data using gramian constraints: Geophysical Research Letters, **39**, doi: https://doi.org/10.1029/2012GL051233.

Zhdanov, M. S., and M. Cuma, 2018, Joint inversion of multimodal data using focusing stabilizers and Gramian constraints: 1430–1434, doi: https://doi.org/10.1190/segam2018-2998495.1.